INTERNATIONAL JOURNAL FOR NUMERICAL METHODS IN FLUIDS
Int. J. Numer. Meth. Fluids 2005; **47**:1293–1299
Published online 17 January 2005 in Wiley InterScience (www.interscience.wiley.com). DOI: 10.1002/fld.848

Multidimensional positive definite advection transport algorithm (MPDATA): an edge-based unstructured-data formulation

Piotr K. Smolarkiewicz[1] and Joanna Szmelter[2,*,†]

[1]*National Center for Atmospheric Research, Boulder, CO 80307, U.S.A.*
[2]*Cranfield University, Royal Military College of Science, Shrivenham, Swindon SN6 8LA, U.K.*

SUMMARY

We report a new development in the area of non-oscillatory transport methods. We derive, discuss, and test the iterative upwind scheme MPDATA in the Finite Volume framework with the edge-based data structure and arbitrary hybrid mesh. MPDATA has proven successful in simulations of geophysical flows using single block, structured cuboidal meshes, while employing continuous invertible mappings to accommodate time-dependent curvilinear domains. Our motivation for the finite-volume formulation and the choice of unstructured meshes is to facilitate the use of MPDATA schemes for a wider range of applications involving complex geometries and/or inhomogeneous anisotropic flows, where mesh adaptivity is advantageous. Our development preserves the signature benefits of the standard Cartesian-mesh MPDATA scheme, i.e. the second-order accuracy, sign-preservation, and a full multidimensionality free of directional-splitting errors. Copyright © 2005 John Wiley & Sons, Ltd.

KEY WORDS: nonoscillatory advection schemes; finite volume methods; unstructured meshes

1. INTRODUCTION

Since its origin in the early eighties [1, 2], MPDATA has evolved from a simple sign-preserving advection scheme to a general, nonoscillatory approach for finite-difference integration of the conservation laws of geophysical fluids on micro-to-planetary scales; cf. Reference [3]. A comprehensive review of MPDATA, including both the underlying concepts and the details of implementation, can be found in Reference [4].

Recently, MPDATA has attracted attention in the context of the monotonically integrated large eddy simulations (MILES), as a high Reynolds number fluid solver with implicit

*Correspondence to: Joanna Szmelter, Cranfield University, Royal Military College of Science, Shrivenham, SN6 8LA, Swindon, U.K.
†E-mail: j.m.szmelter@cranfield.ac.uk

Contract/grant sponsor: U.S.A. Department of Energy

Received 27 April 2004
Revised 27 October 2004
Accepted 27 October 2004

turbulence modelling capability [5–7]. By design, MPDATA relies on iterative application of the upwind scheme, where subsequent iterations compensate for the implicit viscosity of the preceding steps. Thus, it bears an analogy to generalized similarity models, where an estimate of the full unfiltered Navier–Stokes velocity (that enters the subgrid-scale stress tensor) is obtained by an approximate inversion of the filtering operation, i.e. deconvolution [8].

Motivated by the strengths of finite-difference MPDATA,[‡] here we propose a new formulation, in the arbitrary finite-volume framework and hybrid mesh. In MPDATA, as in any Taylor-series based integration method for differential equations, a choice of data structure has a pronounced impact on technical details of the algorithm. Since our aim is a broad range of applications in two and three spatial dimensions with large number of computational cells, we select a general, compact, and computationally efficient edge-based data structure. This contrasts with the approach adopted in Reference [9], where the focus on meteorological applications dictated an unstructured-mesh discretization merely in the horizontal, with the cell-centred and face-centred control-volume staggering of scalar and vector dependent variables, respectively; cf. Reference [10], for a discussion of computational implications of various data structures.

In the following section we show a brief derivation of the finite-volume MPDATA and comment only on key aspects of the implementation. Section 3 concludes the paper with a summary of the benchmark results. The reader interested in engineering the implementation of the theory outlined and compressible flow applications is referred to Reference [11].

2. FINITE-VOLUME MPDATA: BASIC SCHEME

Here, we are concerned with an elementary initial value problem, the advection equation

$$\frac{\partial \Psi}{\partial t} \equiv -\nabla \cdot (\mathbf{v}\Psi) \tag{1}$$

where $\Psi = \Psi(\mathbf{x}, t)$ is a nondiffusive scalar field assumed nonnegative at $t = 0$, and the $\mathbf{v} = \mathbf{v}(\mathbf{x})$ is a prescribed flow assumed stationary and solenoidal. The adopted assumptions merely simplify the presentation; extensions to nonnegative scalar fields and arbitrary flows directly follow the developments for finite-difference MPDATA, cf. Reference [4]. Similarly, we shall disregard the variability of an unstructured grid in time—an assumption easy to relax following finite-difference experience [3]. Integrating (1) over the volume of an arbitrary cell (while employing the Gauss divergence theorem) results in

$$\Psi_i^{n+1} = \Psi_i^n - \frac{\delta t}{\mathscr{V}_i} \sum_{j=1}^{l(i)} F_j^{\perp} S_j \tag{2}$$

Figure 1 shows a face of an arbitrary computational cell containing vertex i, together with the *edge* connecting vertex i with one of its immediate neighbour j; there are $l(i)$ edges connecting the vertex i with its neighbours. S_j refers both to the face *per se* and its surface area. Equation (2) is exact, given Ψ_i^{n+1} and Ψ_i^n are interpreted as the mean values of Ψ

[‡]Although the Cartesian-mesh MPDATA is a particular finite-volume scheme, in general, it derives from finite differencing of the flux-form continuous PDE (1).

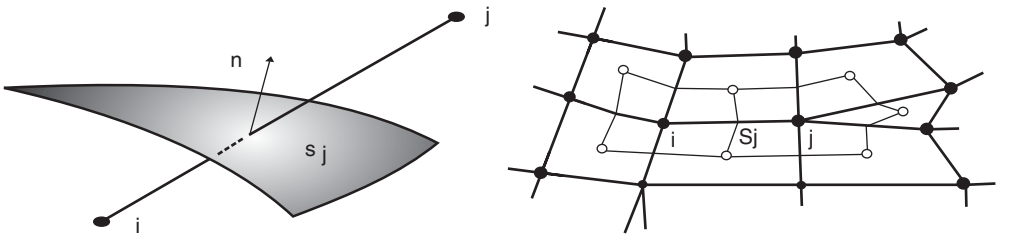

Figure 1. Schematics of an edge piercing a face of an arbitrary 3D cell (left), and of an edge-based median-dual mesh in 2D (right).

within the volume $\mathscr{V}_i$ of the cell containing vertex i, while $F_j^\perp$ is interpreted as the mean normal flux through the cell face S_j averaged over temporal increment δt. The approximation begins with specifying fluxes $F_j^\perp$ in terms of data available on the grid. The finite-volume first-order-accurate upwind scheme—alias donor-cell; hereafter 'upwind' for brevity—assumes

$$F_j^\perp = [v_j^\perp]^+ \Psi_i^n + [v_j^\perp]^- \Psi_j^n; \quad [v]^+ := 0.5(v + |v|), \quad [v]^- := 0.5(v - |v|) \tag{3}$$

where normal velocity $v^\perp \equiv \mathbf{v}\cdot\mathbf{n}$ is evaluated at the face S_j. The non-negative/non-positive parts of $v_j^\perp$ always coincide with outflow/inflow from the ith cell. Given suitably limited δt, via a Courant–Friedrichs–Lewy condition, the upwind scheme exhibits the signature virtues of sign preservation (for arbitrary flows) and *convexity*[§] (if $\nabla\cdot\mathbf{v} \equiv 0$). The sign preservation suffices for the non-linear stability. These apparent strengths of the scheme are offset, however, by the notorious numerical viscosity.

The key idea of MPDATA [1, 2] is to compensate for the truncation error of the upwind scheme by reusing the same upwind algorithm but with a pseudo-velocity defined based on the leading (dissipative) truncation error of the first step. By design, this leads to a scheme that is second-order accurate, yet sign-preserving for arbitrary flows.[¶]

In order to assess the leading truncation error of the finite-volume upwind differencing, we begin with expanding Ψ_i and Ψ_j that enter the definition of the upwind flux in (3) about a point 's_j' along the edge connecting vertices i and j, where the edge intersects the cell face S_j

$$\Psi_i = \Psi\Big|_{s_j} + \frac{\partial\Psi}{\partial r}\Big|_{s_j}(r_i - r_{s_j}) + \mathcal{O}(\delta r^2), \quad \Psi_j = \Psi\Big|_{s_j} + \frac{\partial\Psi}{\partial r}\Big|_{s_j}(r_j - r_{s_j}) + \mathcal{O}(\delta r^2) \tag{4}$$

with r referring to the parametric description of the edge $r(\lambda) = r_i + \lambda(r_j - r_i)$; $\lambda \in [0, 1]$. Now, implementing (4) in the definition of the upwind flux (3), employing the relations $v = [v]^+ + [v]^-$ and $|v| = [v]^+ - [v]^-$ implied by the definitions in (3), and rearranging the terms, results in

$$F_j^\perp = v_j^\perp \Psi\Big|_{s_j}^n + 0.5|v_j^\perp| \frac{\partial\Psi}{\partial r}\Big|_{s_j}^n (r_i - r_j) + 0.5 v_j^\perp \frac{\partial\Psi}{\partial r}\Big|_{s_j}^n (r_i - 2r_{s_j} + r_j) + \mathcal{O}(\delta r^2) \tag{5}$$

[§]The field values are bounded by the surrounding values at the preceding time step.
[¶]Extensions to fully monotone schemes are available [4].

that already reveals the explicit form of the $\mathcal{O}(\delta r)$ error in the approximation (2)–(3). In order to reveal the $\mathcal{O}(\delta t)$ error, it now suffices to expand Ψ^n about $t^{n+1/2}$

$$\Psi\Big|_{s_j}^{n} = \Psi\Big|_{s_j}^{n+1/2} - 0.5\,\frac{\partial\Psi}{\partial t}\Big|_{s_j}^{n+1/2}\delta t + \mathcal{O}(\delta t^2) \tag{6}$$

only in the first term on the rhs of (5). Expanding spatial derivatives (about $t^{n+1/2}$) in the remaining terms is unnecessary, as it would lead to $\mathcal{O}(\delta t\delta r)\sim\mathcal{O}(\delta r^2)$ errors.

For preserving the explicitly forward-in-time (as opposed to centred-in-time) character of the approximation (2)–(3), it is important to express the temporal derivative in (6) in terms of spatial differencing to $\mathcal{O}(\delta t, \delta r)$ at least. Although written in the integral form, (2)–(3) approximate (1) to $\mathcal{O}(\delta r)$ essentially by design. Consequently: (i) viewing (1) as $\partial\Psi/\partial t = -\mathbf{v}\nabla\Psi - \Psi\nabla\cdot\mathbf{v}$, (ii) replacing the temporal derivative in (6) with the rhs of the equation in (i), and (iii) substituting the resulting relation in (5) for $\Psi|_{s_j}^{n}$ in the first term on the rhs results in

$$\begin{aligned} F_j^{\perp} &= v_j^{\perp}\Psi|_{s_j}^{n+1/2} + \text{Error} \\ \text{Error} &= -0.5|v_j^{\perp}|\,\frac{\partial\Psi}{\partial r}\Big|_{s_j}^{*}(r_j - r_i) + 0.5v_j^{\perp}\,\frac{\partial\Psi}{\partial r}\Big|_{s_j}^{*}(r_i - 2r_{s_j} + r_j) \\ &\quad + 0.5\delta t\, v_j^{\perp}(\mathbf{v}\nabla\Psi)|_{s_j}^{*} + 0.5\delta t\, v_j^{\perp}(\Psi\nabla\cdot\mathbf{v})|_{s_j}^{*} + \mathcal{O}(\delta r^2, \delta t^2, \delta t\,\delta r) \end{aligned} \tag{7}$$

The asterisk in lieu of the temporal level in the Error symbolizes either n, $n+\frac{1}{2}$, or $n+1$, as any of these temporal positions can be considered without affecting the form or the order of Error. The result in (7) states that the upwind flux in (3) can be decomposed into a time-centred flux through the face and the $\mathcal{O}(\delta r, \delta t)$ flux of a predominantly Fickian character.

As with finite differences, finite-volume MPDATA consists of two upwind iterations (2)–(3). In the first iteration, the input field and flow velocity, Ψ and $\mathbf{v}$, are those from the preceding time step t^n. In the second (corrective) iteration, the input field Ψ is the result of the preceding upwind iteration and the pseudo velocity $\widetilde{v}\equiv -(1/\Psi)\text{Error}$. In particular,

$$\begin{aligned} \widetilde{v}_j^{\perp} &= 0.5|v_j^{\perp}|\,\left(\frac{1}{\Psi}\,\frac{\partial\Psi}{\partial r}\right)\Big|_{s_j}^{*}(r_j - r_i) - 0.5v_j^{\perp}\,\left(\frac{1}{\Psi}\,\frac{\partial\Psi}{\partial r}\right)\Big|_{s_j}^{*}(r_i - 2r_{s_j} + r_j) \\ &\quad -0.5\delta t\, v_j^{\perp}\,\left(\mathbf{v}\,\frac{1}{\Psi}\,\nabla\Psi\right)\Big|_{s_j}^{*} - 0.5\delta t\, v_j^{\perp}(\nabla\cdot\mathbf{v})|_{s_j}^{*} \end{aligned} \tag{8}$$

with the asterisk indicating now the first-order estimate of the $n+1$ solution from the preceding upwind iteration. The entire process of estimating the residual error and compensating it can be continued, iteration after iteration, reducing the magnitude of the truncation error, yet the single corrective iteration suffices for the second-order accuracy.

The outlined procedure conveys the essence of the finite-volume MPDATA in abstraction from particularities of spatial discretization. Notwithstanding, the general form of the pseudo velocity (8) deserves a comment because it offers much guidance on how to design effective

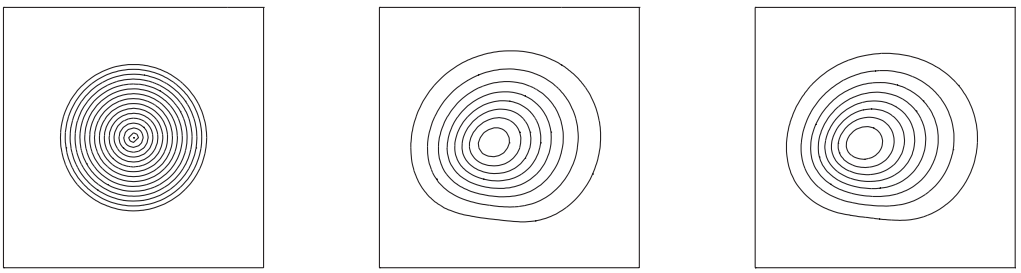

Figure 2. Isolines of cone advected through six rotations around the centre of the lower frame (only a quarter of the domain is shown). The contour interval is 0.25, and the zero contour line is not shown. Left plate, the analytic solution; centre plate, the FV MPDATA on a regular square-mesh; right plate, as in the centre but for a triangular mesh.

implementations, and because it involves a few subtleties compared to the forms previously published in the context of finite differences.

The first term on the rhs of (8) is well known from finite-difference theory, and straightforward to approximate on unstructured meshes. The second term—hereafter the 'mesh-skewness' term—is new. However, since it vanishes wherever the cell face is at the midpoint of the edge, it can be set to zero with an adequate discretization. In particular, in our implementation we use the median dual finite volume discretization [12] that, by design, allows for a mean curvature of the face and cancels out the mesh-skewness error; see Figure 1 for a schematic. The third term, proportional to $(\mathbf{v}\Psi^{-1}\nabla\Psi)$, is the most cumbersome. On an orthogonal mesh it becomes naturally decomposed into convective derivatives normal and tangential to cell faces. In a general finite-volume framework, however, the advantages of such a strategy become either irrelevant or uncertain. Following Bacon *et al.* [9], here we shall evaluate the entire convective derivative in terms of the Cartesian components.[‖] Finally, the $\sim\nabla\cdot\mathbf{v}$ is irrelevant in this paper. In the solenoidal flows assumed, it vanishes identically in the first corrective iteration of MPDATA, whereas in subsequent iterations it enters as $\mathcal{O}(\delta t^2)$ and is thus negligible [2]. In arbitrary flows, its accommodation follows straightforwardly the finite-difference developments [3, 4].

3. RESULTS

Herein, we illustrate the performance of the finite-volume MPDATA using a standard solid-body rotation test [1, 2, 4]. A cone of base radius 15 and height 4, centred initially at $(75, 50)$, is rotating counterclockwise around the centre of a $[0, 100]\times[0, 100]$ domain with the angular velocity $\omega = 0.1$. Figure 2 displays the isolines of the exact result and two FV MPDATA solutions after 6 rotations. The solution in the central plate uses 10^4 squared cells, whereas

[‖] As with finite-difference MPDATA, we always assure that denominators and numerators in approximations to all $\sim\Psi^{-1}\partial\Psi$ factors in (8) use the same elements, thereby resulting in the ratios of the $\sum\pm\Psi/\sum\Psi$ type, whose absolute values never exceed unity for nonnegative Ψ, cf. Reference [11].

Table I. Error norms for solid-body rotation test using finite-volume and finite-difference MPDATA; the classical upwind and centred-in-time-and-space leapfrog schemes are included for reference.

Scheme	Max	Min	L_2
MPDATA FD	2.18	0	0.47×10^{-3}
MPDATA FV squares	2.18	0	0.47×10^{-3}
MPDATA FV triangles	2.00	0	0.54×10^{-3}
Upwind FD	0.27	0	1.21×10^{-3}
Upwind FV squares	0.28	0	1.04×10^{-3}
Upwind FV triangles	0.25	0	1.06×10^{-3}
Leapfrog FD	3.16	−0.62	0.62×10^{-3}
Leapfrog FV squares	3.11	−0.67	0.64×10^{-3}
Leapfrog FV triangles	3.11	−0.69	0.65×10^{-3}

the solution in the right plate uses a triangular grid with a similar number and distribution of points. For reference, all parameters of the test and of the display are selected identical to those in Figure 1 of Reference [4]. The accuracy of the results displayed is quantified in Table I, where the corresponding values for the classical upwind and centred-in-time-and-space leapfrog schemes are included for the sake of reference. Noteworthy, we verified (not shown) that MPDATA and leapfrog achieve the same convergence rates for both formulations and grids employed.

ACKNOWLEDGEMENTS

Comments from Anna Crowley, Len Margolin, and two anonymous referees helped to improve the presentation. This work was supported in part by the U.S.A. Department of Energy 'Climate Change Prediction Program' (CCPP) research initiative.

REFERENCES

1. Smolarkiewicz PK. A simple positive definite advection scheme with small implicit diffusion. *Monthly Weather Review* 1983; **111**:479–486.
2. Smolarkiewicz PK. A fully multidimensional positive definite advection transport algorithm with small implicit diffusion. *Journal of Computational Physics* 1984; **54**:325–362.
3. Smolarkiewicz PK, Prusa JM. Forward-in-time differencing for fluids: simulation of geophysical turbulence. In *Turbulent Flow Computation*, Drikakis D, Guertz BJ (eds). Kluwer Academic Publishers: Dordrecht, 2002; 207–240.
4. Smolarkiewicz PK, Margolin LG. MPDATA: a finite-difference solver for geophysical flows. *Journal of Computational Physics* 1998; **140**:459–480.
5. Domaradzki JA, Xiao Z, Smolarkiewicz PK. Effective eddy viscosities in implicit large eddy simulations of turbulent flows. *Physics of Fluids* 2003; **15**:3890–3893.
6. Margolin LG, Rider WJ. A rationale for implicit turbulence modeling. *International Journal for Numerical Methods in Fluids* 2002; **39**:821–841.
7. Margolin LG, Smolarkiewicz PK, Wyszogrodzki AA. Implicit turbulence modeling for high Reynolds number flows. *Journal of Fluids Engineering* 2002; **124**:862–867.
8. Domaradzki JA, Adams NA. Direct modelling of subgrid scales of turbulence in large eddy simulation. *Journal of Turbulence* 2002; **3**:1–19.
9. Bacon DP *et al*. A dynamically adapting weather and dispersion model: the operational environment model with grid adaptivity (OMEGA). *Monthly Weather Review* 2000; **128**:2044–2076.

10. Mavriplis DJ. Three dimensional unstructured multigrid for the Euler equations. *AIAA Journal* 1992; **30**(7): 1753–1761.
11. Szmelter J, Smolarkiewicz PK. A low-implicit-diffusion flow solver for unstructured meshes. *AIAA 2005-0321 Paper*.
12. Barth TJ. Aspects of unstructured grids and finite volume solvers for the Euler and Navier–Stokes equations. *Special Course on Unstructured Grid Methods for Advection Dominated Flows, AGARD. Report 787*, 1992; 6.1–6.61.

